ARTICLE TEMPLATE

Neuro-adaptive Sliding Mode Control for Underground Coal Gasification Energy Conversion Process

Mutahir Khattak[a], Ali Arshad Uppal[a], Qudrat Khan[b], Aamer Iqbal Bhatti[c], Yazan M. Alsmadi[d], Vadim I. Utkin[e] and Issac Chairez[f]

[a] Department of Electrical and Computer Engineering, COMSATS University Islamabad, Islamabad, Pakistan; [b]Center for Advanced Studies in Telecommunications, COMSATS University Isamabad, Islamabad, Pakistan; [c]Department of Electrical Engineering, Capital University of Science and Technology, Islamabad, Pakistan; [d]Electrical Engineering Department, Jordan University of Science and Technology, Irbid, Jordan; [e]Electrical and Computer Engineering Department, The Ohio State University, Columbus, OH, USA; [f]UPIBI-Instituto Politcnico Nacional Mexico City, Mexico;

ARTICLE HISTORY
Compiled January 20, 2020

ABSTRACT
The control design of a non-linear and infinite dimensional underground coal gasication (UCG) process is a challenging task. As the process takes place in-situ, and no physical insight is available, so it is either very expensive or difficult to measure all the essential process parameters, which further complicates the control design. In this paper, a robust neuro-adaptive sliding mode control (NASMC) algorithm is designed for an infinite dimensional model of the UCG process in order to maintain a desired constant heating value. The unknown model parameters used in the controller design are estimated using the feed forward neural network (FFNN). Moreover, the controller also requires time derivatives of the measured model parameters, which are estimated by uniform robust exact differentiator (URED). As the relative degree of the process output with respect to the input is zero, therefore, in order to apply the SMC approach, the relative degree is increased to one. Consequently, the control input bears a time derivative which is needed to be filtered once given to the plant. This approach maintains the output at the desired level and provides insensitivity to input disturbance and model uncertainties. A comparison is also made between NASMC and an already designed conventional SMC. The simulation results show that NASMC exhibits better performance as compared to the conservative SMC design.

KEYWORDS
Relative degree, neuro-adaptive sliding mode control (NASMC), feed forward neural network (FFNN), uniform robust exact differentiator (URED), underground coal gasification (UCG) and energy conversion systems

1. Introduction

Coal plays a pivotal role in fulfilling the world's energy requirements. Moreover, it is the leading fuel for electricity production and its consumption is increased by 25 million tonnes of oil equivalent (mtoe) since 2013 (Petroleum, 2018). Coal can be chemically

CONTACT Vadim Utkin. Email: utkin.2@osu.edu

converted into useful synthetic gas (syngas) either by gasifiying it on the surface or by utilizing the underground coal gasification (UCG) technology. In surface gasification a number of steps are involved which mainly include, mining and purification of coal, followed by its gasification in specially designed chambers to produce synthesis or syngas (Bell et al., 2011). On the other hand, UCG produces syngas at low to medium heating value by gasifying the coal in-situ. Thus, UCG turns into the main choice for low rank coal (heating value less than 12 MJ/kg) (Van der Riet, 2008), which is monetarily infeasible for mining.

The process of UCG starts by drilling injection and production wells, which are directly perforated into the coal seam, trailed by the establishment of a permeable channel between the wells. Prior to the gasification process, the coal seam is kindled to set the initial dissemination for the reactors temperature, which is very important in the success of the UCG process. The oxidants (air and steam ($H_2O(g)$) or Oxygen (O_2) or only air) are injected via the injection well into the coal seam, which chemically react with already kindled coal to produce syngas which is collected from the production well. The syngas is normally a mixture of hydrogen (H_2), carbon monoxide (CO), methane (CH_4) and traces of higher hydrocarbons (C_nH_m), which can be used as a major source for power generation, industrial heating and for the production of liquid fuels (Khadse et al., 2006; Perkins, 2005).

In order to increase the efficiency of a UCG process, a control system can be designed, which is capable of maintaining heating value of the product gases at the desired level for a longer period of time (Uppal et al., 2014). In literature both model-free and model-based control strategies have been explored for the UCG process. In (Kostúr and Kačúr, 2008; Kostur and Kacur, 2011, 2017), different model-free control techniques have been implemented on a lab scale UCG process to control heating value and composition of product gases, and other important parameters of the process. However, the control of actual UCG process is a formidable task, especially considering the unavailability of the measurements of some essential model parameters. Since UCG process takes place underground and no physical insight is available, so it is very expensive and difficult to measure the necessary model parameters of the process by installing sensors at different locations of the reactor. The only available measurements of the whole process are the flow rate and composition of the product gas mixture. In this scenario a detailed model of the UCG process is of paramount importance for the analysis and control of UCG process (Uppal, 2016).

The model-based control heavily relies on the selection of a suitable mathematical model of the process. There is always a trade-off between the accuracy of the model and ease of the controller design (Uppal, 2016). Owing to their complex dynamics, most of the available UCG models can not be employed for the model-based control easily. Two control-oriented models of UCG have been reported in the literature. A simplified nonlinear ODEs based model (Arshad et al., 2012), derived from (Thorsness and Rozsa, 1978) and (Winslow, 1977). The model ignores the dynamics of the process with respect to length of the reactor. The simplified model is used to design a conventional sliding mode control (SMC), cf. (Arshad et al., 2012), an integral SMC, cf. (Uppal et al., 2018b) and a dynamic integral SMC, cf. (Uppal et al., 2019) to keep the heating value at the desired level. In (Arshad et al., 2012) it has been assumed that all the state variables are available for controller design, which is practically impossible. Therefore, in (Uppal et al., 2018b, 2019), a gain-scheduled modified Utkin observer is designed to reconstruct the unknown states, followed by integral and dynamic integral SMC designs, respectively. In (Chaudhry et al., 2018), the model of (Arshad et al., 2012) is linearized around an operating point of interest. The model is then employed to

design a robust multi-objective H_2/H_∞ controller for maintaining a desired level of the heating value. Another control-oriented model of UCG has been proposed in (Uppal et al., 2014), which is based on the model of (Thorsness and Rozsa, 1978). The model gives a better representation of the UCG process as compared to the model in (Arshad et al., 2012). The infinite dimensional, pseudo-steady state model is comprised of PDEs for solids and space dependent ODEs for gases. Two different control techniques have been designed for the model, a super-twisting based SMC, cf. (Uppal et al., 2015) and a conventional SMC, cf. (Uppal et al., 2018a). The gains for both the controllers are computed by finding the upper bounds of the unknown functions of the model in (Uppal et al., 2014), by using rigorous simulation study. In order to avoid a conservative control design cf. (Uppal et al., 2018a, 2015), it is more convenient to estimate the important model parameters utilizing the available measurements. For such purpose many parameter estimation techniques are available. However, for a complex and highly nonlinear UCG process, the artificial neural networks (ANNs) based parameter estimation technique, cf. (Bhatti et al., 1996; Chauhan and Singh, 2017; Hagan et al., 2002; Khan and Akmeliawati, 2017; Rostami et al., 2018) becomes a suitable candidate.

The integration of ANNs and sliding modes has been considered in diverse modeling and control contexts, cf. (Chairez et al., 2006; Ertugrul and Kaynak, 2000; Nied et al., 2007). Much of such approaches reported a class of pseudo robust-adaptive controller which has not been clearly motivated, cf. (and and, 2002; Bari et al., 2005; Bouhali and Boudjedir, 2011; PARMA et al., 1999). The application of the controller proposed in this study considers a different application of the ANNs as part of a sliding mode controller for an Underground Coal Gasification Energy Conversion Process. In this case, the time-derivative of the sliding surface depends on some uncertain terms which are functionally connected with some measurable inputs at the border of the spatial domain of the conversion process. This functional relationship is approximated with a suitable ANN which is substituted into the control design. Moreover, the proposed approximation relaxes some modeling assumptions used in the regular model of the process that must be controlled.

Therefore, in this work the model of (Uppal et al., 2014) is employed to estimate the unknown parameters, which are nonlinear functions of measured and unmeasured system variables, using the feed-forward neural network (FFNN). The parameters are then used for designing SMC for maintaining the desired heating value. Consequently, the neuro-adaptive sliding mode control (NASMC) yields less conservative controller gains, improving the performance of the closed loop system. Moreover, the robustness is also improved by estimating these non-linear functions along with relaxation of these functions to be bounded (Rostami et al., 2018). The unknown model parameters are also dependent on time derivatives of the measured concentrations. It has been observed that the time differentiation of discrete samples of measured data is "utmost important " problem. The trade-off between exactness and robustness with respect to the input sampling data and noise is the major issue in time differentiator design (Cruz-Zavala et al., 2011). Also, the draw back of traditional differentiators, used in many applications, is the asymptotic convergence, when the norm of initial conditions of the differentiation error grows unboundedly. Therefore, to overcome this problem, the design of such a differentiator is required, which converges exactly and robustly in a finite time, independent of initial differentiator error and despite of bounded uncertainties. One such differentiator is the uniform robust exact differentiator (URED) (Cruz-Zavala et al., 2011). After estimating the unknown model parameters using measurements and their time derivatives, NASMC is designed.

The simulation results show that NASMC yields better performance in the presence of modeling uncertainties and external disturbance as compared to the SMC design in (Uppal et al., 2018a).

This study provides a novel adaptive compensated sliding mode controller for a class of underground coal gasification energy conversion process. The selected combination of sliding mode control and the adaptive estimation based on ANN enforces the output value of the system to track reference values, which can be obtained as a result of precise estimation of the unknown parameters as well as their derivatives, which are estimated with the application of a set of robust differentiators. The realization of this controller also uses a synthetic increment of the relative degree of the sliding surface with respect to the controller, which provides a smoother variation of the control approach. The outcomes of this study demonstrate that the application of the adaptive compensated controller may produce a regulated composition of the energetic process.

The remainder of this paper is structured as follows: In Section 2 the problem statement and the control-oriented model is developed with the help of certain assumptions. The design of NASMC and the non-linear parameter estimation using NN technique are demonstrated in Section 3 and 4 respectively. In Section 5 numerical solution of the closed loop system is explained. Section 6 presents the simulations results, and this paper is concluded in Section 7.

2. Mathematical Model of UCG Process

In this work 1D packed bed model of (Uppal et al., 2014) is employed to design the NASMC for the UCG process. The schematic of the process is shown in Fig. 1.

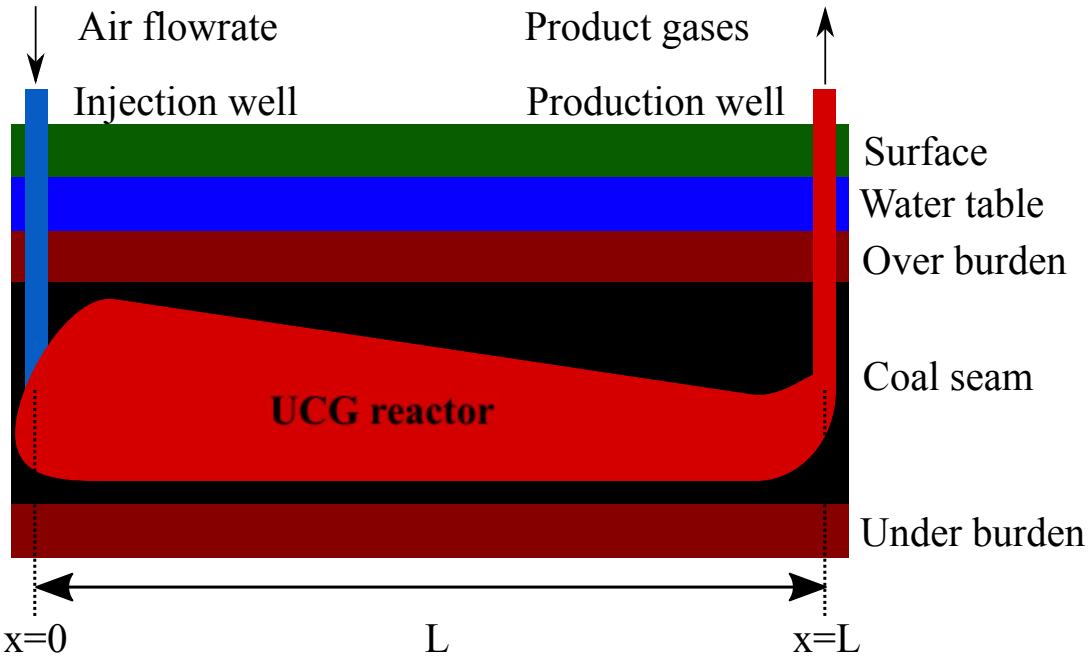

Figure 1. Schematic of UCG process (Uppal et al., 2014)

The mass and energy balances of coal and char are modeled as 1D PDEs in time

and space, which are given as

$$\frac{\partial \rho_1}{\partial t} = -M_1 R_1, \tag{1}$$
$$\rho_1\left(0,x\right) = \rho_{1_0}(x),\ 0 \le x \le L,$$
$$\frac{\partial \rho_2}{\partial t} = M_2\Big(a_{s_{2,1}} R_1 - R_2(u) - R_3(u)\Big), \tag{2}$$
$$\rho_2\left(0,x\right) = \rho_{2_0}(x),\ 0 \le x \le L,$$
$$\frac{\partial T_s}{\partial t} = \frac{\frac{\partial}{\partial x}\Big((1-\varphi)k\frac{\partial T_s}{\partial x}\Big) + h(T_g - T_s) - \sum_{j=1}^{3} q_j R_j}{(cp_1\rho_1 + cp_2\rho_2)}, \tag{3}$$
$$T_s\left(0,x\right) = T_{s_0}(x), \quad 0 \le x \le L,$$
$$\frac{\partial T_s}{\partial x}\left(t,0\right) = \frac{\partial T_s}{\partial x}\left(t,L\right) = 0, \quad t \ge 0.$$

The description of the model parameters is given in Table. 1.

Due to pseudo steady-state assumption, the mass and energy balances of the gases are represented by ODEs in length domain

$$\frac{dC_i}{dx} = \frac{1}{v_g}(-C_i\frac{dv_g}{dx} + \sum_{j=1}^{3} a_{s_{ij}} R_j), \tag{4}$$
$$C_i(x=0) = \Big[0\ 0\ 0\ 0\ 0.79\tfrac{u}{v_{g_0}}\ 0.21\tfrac{u}{v_{g_0}}\ 0\ \tfrac{\delta}{v_{g_0}}\Big]^T,$$
$$\frac{dT_g}{dx} = -\frac{h}{v_g C_g}(T_g - T_s), \tag{5}$$
$$T_g(x=0) = T_{g_0},$$
$$\frac{dP}{dx} = -\frac{v_g \mu}{2K}, \tag{6}$$
$$P(x=0) = P_0,$$
$$\frac{dv_g}{dx} = -\frac{v_g}{P}\frac{dP}{dx} + \frac{v_g}{T_g}\frac{dT_g}{dx} + \frac{RT_g}{P}\sum_{i=1}^{8}\sum_{j=1}^{3} a_{s_{ij}} R_j, \tag{7}$$
$$v_g(x=0) = v_{g_0}.$$

where $C_i,\ i \in \{1,\ldots,8\}$ represents the concentration of CO, CO_2, H_2, CH_4, N_2, O_2, Tar and H_2O within the UCG reactor.

According to (Uppal et al., 2014), the chemical kinetics of the process is mainly governed by three chemical reactions, which are given in Table. 2. The rates of the chemical reactions are expressed as

Table 1. LIST Of SYMBOLS

Sr.#	Symbol	Description
1.	ρ_1, ρ_2	densities of coal and char (g/cm^3)
2.	M_1, M_2	Molecular weights of coal and char (g/mol)
3.	$a_{s_{i,j}}$, $a_{i,j}$	Stoichiometric coefficients of solids and gases solid in jth reaction
4.	R_j	Rate of jth chemical reaction (mol/cm^3/s)
5.	T_s, T_g	Solid and gas temperatures (K)
6.	φ	Porosity of coal bed
7.	k	Effective thermal conductivity of solids (cal/cm/s/K)
8.	h	Heat transfer coefficient (cal/s/K/cm^3)
9.	C_s	Total solid phase heat capacity (cal/K/cm^3)
10.	C_g	Total gas phase heat capacity (cal/mol/K)
11.	q_i	Heat of ith reaction (cal/mol)
12.	P, v_g	Pressure (atm) and gas velocity (cm/s)
13.	H_g	Gas phase heat source ($J/s/cm^3$)
14.	K, μ	Gas permeability (cm^2) and viscosity (Pa.s)
15.	R	Universal gas constant (cm^{3}atm/mol/K)
16.	L	Reactor length 2500 cm
17.	k_y	Mass transfer coefficient (mol/cm^3/s)
18.	u	Input air flow rate (mol/cm^2/s)
19.	δ	flow rate of steam (mol/cm^2/s)
20.	H_v	Heating Value of gases (KJ/mol^3)
21.	C_i	Concentration of ith gas (mol/cm^3)

$$R_1 = 5\frac{\rho_1}{M_1}\exp\left(\frac{-6039}{T_s}\right), \tag{8}$$

$$R_2 = \frac{R_{c_2} k_y y_{O_2}}{R_{c_2} + k_y y_{O_2}}, \tag{9}$$

$$R_{c_2} = \frac{9.55\times 10^8 \rho_2 y_{O_2} P \exp\left(\frac{-22142}{T_s}\right) {T_s}^{-0.5}}{M_2},$$

$$R_3 = \frac{R_{c_3} k_y y_{H_2O}}{R_{c_3} + k_y y_{H_2O}}, \tag{10}$$

$$R_{c_3} = \frac{{R_{c_3}}^+}{y_{H_2O}}\left(y_{H_2O} - \frac{y_{CO} y_{H_2}}{K_{E_3}}\right),$$

$${R_{c_3}}^+ = \frac{\rho_2 y_{H_2O}^2 P^2 \exp\left(5.052 - \frac{12908}{\tilde{T}}\right)}{M_2\left(y_{H_2O}P + \exp\left(-22.216 + \frac{24880}{\tilde{T}}\right)\right)^2}.$$

where y_{O_2}, y_{H_2O}, y_{CO} and y_{H_2} are internal molar fractions of O_2, H_2O, CO and H_2O along x respectively. The internal molar fraction of the gas i is computed as

$$y_i = \frac{C_i}{C_T},$$
$$C_T = \sum_{i=1}^{8} C_i.$$

Table 2. Chemical reactions considered in the model

Sr	Chemical equations
1.	**Pyrolysis**
	$CH_aO_b \xrightarrow{R_1} a_{s_{2,1}} CH_{\bar{a}}O_{\bar{b}} + a_{1,1}CO + a_{2,1}CO_2 + a_{3,1}H_2 + a_{4,1}H_2O + a_{5,1}CH_4 + a_{8,1}C_9H_c$
2.	**Char Oxidation**
	$CH_{\bar{a}}O_{\bar{b}} + a_{7,2}O_2 \xrightarrow{R_2} a_{2,2}CO_2 + a_{4,2}H_2O$
3.	**Steam gasification**
	$CH_{\bar{a}}O_{\bar{b}} + a_{4,3}H_2O \xleftrightarrow{R_3} a_{1,3}CO + a_{3,3}H_2$

CH_aO_b, $CH_{\bar{a}}O_{\bar{b}}$ and C_9H_cin Table. 2 represent molecular formulas for coal, char and Tar respectively.

As shown in Fig. 1, air at particular flow-rate enters the injection well ($x = 0$), and the product gases are recovered from the production well ($x = L$). After the removal of H_2O, the gas mixture is sent to the gas analyzer, where the concentration of the gases is measured. Based on the measurement, the percentage volumetric content (molar fraction) of the gases (except H_2O) is computed (Uppal et al., 2014). Hence, the measurement vector $\vec{y}_m$ is given by

$$\begin{aligned}\vec{y}_m = &\big[C_{\mathrm{CO}}(L)C_{\mathrm{CO_2}}(L)C_{\mathrm{H_2}}(L)C_{\mathrm{CH_4}}(L) \\ &C_{\mathrm{N_2}}(L)C_{\mathrm{O_2}}(L)C_{\mathrm{Tar}}(L)\big]^T .\end{aligned} \tag{11}$$

The heating value is calculated as

$$H_v = H_{\mathrm{CO}}\Omega_{\mathrm{CO}} + H_{\mathrm{H_2}}\Omega_{\mathrm{H_2}} + H_{\mathrm{CH_4}}\Omega_{\mathrm{CH_4}} + H_{\mathrm{Tar}}\Omega_{\mathrm{Tar}}, \tag{12}$$

where $H_i, i \in \{\mathrm{CO}, \mathrm{H_2}, \mathrm{CH_4}, \mathrm{C_nH_m}\}$ is the combustion heat (KJ/mol) of gas i, $\mathrm{C_nH_m}$ represents higher hydrocarbons and Ω_i is the molar fraction of the gases, charaterized by the ratio

$$\Omega_i = 100\frac{C_i(x)}{C_m(x)}\bigg|_{x=L},$$
$$C_m = \sum_{j=1}^{7} \vec{y}_m(j).$$

where C_m is the sum of concentration of all the gases (except H_2O). It is pertinent to mention that Tar is a pseudo specie, introduced to balance the coal pyrolysis reaction. It also accounts for the higher hydrocarbons, which actually contribute in H_v.

The controller design for maintaining a desired level of H_v is discussed in the subsequent section.

3. Controller Design

To maintain H_v at a desired constant level (H_{v_r}) a simple sliding surface is selected

$$s = H_{v_r} - H_v. \tag{13}$$

After the establishment of sliding mode $s = 0$, the desired objective ($H_v = H_{v_r}$) can be achieved.

Before designing the control input u, which enforces the sliding mode in the manifold $s = 0$, it is important to investigate the relationship between H_v and the input u. In order to simplify the controller design it is assumed that the gas velocity v_g is constant along x (Uppal et al., 2018a). As N_2 is an inert gas, so it doesn't participate in any chemical reaction. Therefore, according to Eq. (4) $C_{N_2}(x = L) = C_{N_2}(x = 0) = 0.79\frac{u}{v_{g_0}}$ and H_v can be rewritten as

$$\begin{aligned} H_v &= 100\frac{\mathcal{N}}{\mathcal{D} + 0.79\frac{u}{v_{g_0}}}, \\ \mathcal{N} &= H_{\mathrm{CO}}C_{\mathrm{CO}} + H_{\mathrm{H_2}}C_{\mathrm{H_2}} + H_{\mathrm{CH_4}}C_{\mathrm{CH_4}} + H_{\mathrm{Tar}}C_{\mathrm{Tar}}\Big|_{x=L}, \\ \mathcal{D} &= C_{\mathrm{CO}} + C_{\mathrm{CO_2}} + C_{\mathrm{H_2}} + C_{\mathrm{CH_4}} + C_{\mathrm{O_2}} + C_{\mathrm{Tar}}\Big|_{x=L}. \end{aligned} \tag{14}$$

As the relative degree of H_v and hence s with respect to u is zero, so the trivial control design is not an appropriate option. To solve this problem, we try to enforce sliding mode and inserting integrator in the input, such that $\dot{u} = \mu$. The time derivative of sliding variable s is

$$\dot{s} = \dot{H}_{v_r} - \dot{H}_v. \tag{15}$$

Taking time derivative of Eq. (14) and using $\dot{H}_{v_r} = 0$ (desired value is constant), Eq. (15) becomes

$$\begin{aligned} \dot{s} &= \theta + \phi\mu, \\ \theta &= 100\frac{\mathcal{N}\dot{\mathcal{D}} - \dot{\mathcal{N}}\left(\mathcal{D} + \alpha u\right)}{\left(\mathcal{D} + \alpha u\right)^2}, \\ \phi &= 100\frac{\mathcal{N}\alpha}{\left(\mathcal{D} + \alpha u\right)^2}, \end{aligned} \tag{16}$$

where $\alpha = \frac{0.79}{v_{g_0}}$ is a constant.

Here, it is important to discuss the parameters $\theta = \theta_0 + \Delta\theta$ and $\phi = \phi_0 + \Delta\phi$, where $||\Delta\theta|| \leq \Theta \in \mathbb{R}^+$ and $||\Delta\phi|| \leq \Phi \in \mathbb{R}^+$ are uncertain but bounded terms. The uncertainties in θ and ϕ originate due the assumptions considered in this work, which include constant gas velocity (the actual gas velocity is given by Eq. (7)) and assuming that Tar only accounts for the higher-hydrocarbons. Moreover, the model limitations discussed in (Uppal et al., 2014) also add to the uncertainties in θ and ϕ.

The sliding mode is enforced in finite time by considering the following reaching law

$$\dot{s} = -\mathcal{K}\,\mathrm{sign}(s), \tag{17}$$

where $\mathcal{K} \in \mathbb{R}^+$ is the discontinuous sliding mode gain.

The comparison of Eqs.(16) and 17 results in following control law

$$\dot{u} = -\frac{1}{\phi}\Big(\theta + \mathcal{K}\,\mathrm{sign}(s)\Big) \tag{18}$$

3.1. Existence of Sliding Mode

For the stability and existence of sliding mode in the presence of input disturbance, a positive definite Lyapunov function is selected

$$V = \frac{1}{2}s^2. \tag{19}$$

The time derivative of the Lyapunov function is given as

$$\begin{aligned}
\dot{V} &= s\dot{s}, \\
&= s\left(\theta + \phi\dot{u} + \beta\dot{\delta}\right), \\
&= s\left(-\mathcal{K}\,\mathrm{sign}(s) + \beta\dot{\delta}\right), \\
&\leq -|s|\Big(\mathcal{K} - \mathcal{B}\Pi\Big),
\end{aligned} \tag{20}$$

where $||\beta|| \leq \mathcal{B}$ and $||\dot{\delta}|| \leq \Pi$.

Now, if $\mathcal{K} > \kappa + \mathcal{B}\Omega$ with $\kappa > 0$, then the time derivative of the Lyapunov function becomes negative definite

$$\dot{V} \leq -\kappa|s|, \tag{21}$$

and sliding mode exists in finite time (Edwards and Spurgeon, 1998).

After the enforcement of the sliding mode $s = 0$ in finite time, the PDES in Eqs. (1)–(3) constitute the zero dynamics of the process. It has been already proved in (Uppal et al., 2018a) that the zero dynamics is bounded. Therefore, the control design is possible.

From Eq. (18) it is evident that controller utilizes the terms θ and ϕ despite they are uncertain. It is discussed in the subsequent section that these parameters are estimated using FFNN.

4. NN based non-linear Parameter estimation

In order to formulate the target values of θ and ϕ, the time derivatives of the elements of $\vec{y}_m$ (except $C_{N_2}(L)$), cf. Eq. (11) are required, which are computed by designing URED for each concentration of gas. URED is designed particularly to estimate the robust and exact time derivatives as compared to the traditional differentiation approach. The detailed description of the design process of URED for concentrations of gases is explained in the following subsection.

4.1. URED design for concentration of gases

Consider the input signal C_i to be differentiated, with $\varsigma_0 = C_i$ and $\varsigma_1 = \dot{C}_i$ representing states of the second order system

$$\begin{aligned} \dot{\varsigma}_0 &= \varsigma_1, \\ \dot{\varsigma}_1 &= \ddot{C}_i. \end{aligned}$$

To construct an URED with a prescribed finite time convergence, independent of the initial conditions, which gives a robust estimation of $\dot{C}_i$, by using only the measurement of input signal C_i, following method is adopted. Let $\sigma_0 = z_0 - \varsigma_0$ be the difference between the estimated and actual value of the signal to be differentiated, respectively. Now by using generalized super twisting algorithm (GSTA) the following representation is obtain for URED scheme

$$\begin{aligned} \dot{z}_0 &= -k_1 \xi_1(\sigma_0) + z_1, \\ \dot{z}_1 &= -k_2 \xi_2(\sigma_0), \end{aligned} \tag{22}$$

where, z_0 and z_1 are the estimates of C_i and $\dot{C}_i$ respectively, $k_1,\ k_2 \in \mathbb{R}^+$ are the gains to be designed and the functions ξ_1 and ξ_2 are given by

$$\begin{aligned} \xi_1(\sigma_0) &= \mid \sigma_0 \mid^{1/2} \operatorname{sign}(\sigma_0) + \mu \mid \sigma_0 \mid^{3/2} \operatorname{sign}(\sigma_0), \\ \xi_2(\sigma_0) &= \frac{1}{2} \operatorname{sign}(\sigma_0) + 2\mu\sigma_0 + \frac{3}{2}\mu^2 \mid \sigma_0 \mid^2 \operatorname{sign}(\sigma_0), \end{aligned}$$

where $\mu \geq 0$ is a scalar.

The system given by Eq. (22), representing the URED is implemented in MATLAB by using the following difference equations

$$z_0(t+dt) = z_0(t) + \big(-k_1\xi_1(\sigma_0) + z_1(t)\big)dt,$$
$$z_1(t+dt) = z_1(t) + \big(-k_2\xi_2(\sigma_0)\big)dt,$$

where dt is sampling time of the numerical solution.

4.1.1. URED Simulation Results

For simulations, $k_1 = 5e-5$, $k_2 = 1e-9$, $\mu = 4e-5$ and $z^T(0) = [0 \quad 0]$. The URED results for the time derivatives of the concentrations of $CO, CO_2, H_2, CH_4, O_2, Tar$ at $x = L$ are shown in Fig. 2 Moreover, a comparison is also carried out between the time derivatives obtained from URED and MATLAB. It can be seen from the results that response of URED is very smooth as compared to the time derivatives obtained from Simulink.

4.2. Parameter Estimation Using Multilayer Feed-Forward NN

For the function estimation problem in NN, the training set includes one or more explanatory variables (independent variables) and a set of response variables (dependent variables). Therefore, the NN learns to create a mapping between response variables and explanatory variables, cf. (Rostami et al., 2018) and (Gautam, 2016). Because the mapping between θ or ϕ and the concentration of gases is highly non-linear, so a multilayer perceptron (MLP) NN is needed to learn the non-linear mapping. One such technique is multilayer feed-forward neural network (MLFFNN), cf. (Bhatti et al., 1996) and (Ghunem et al., 2012).

It is a reality that the MLP NN with one hidden layer can be efficient for any particular non-linear estimation problem. Therefore, the MLFFNN with one hidden layer is proposed with the schematic diagram of θ and ϕ shown in Fig. 3.

The input to the network are the concentrations of $CO, CO_2, H_2, CH_4, O_2, Tar$ and airflow rate u. The samples in the input layer being multiplied by scalar weighted connections are sent to hidden layer. The hidden layer computes its net activation as

$$a_j = \sum_{i=1}^{l_0} w_{ji}\, p_i + b_{jo}, \tag{23}$$

where $i = 1, 2, \ldots, l_0$ and $j = 1, 2, \ldots, h_0$, l_0 and j_0 represent the number of inputs to the hidden layer and the hidden layer nodes, respectively, p_i is the input of the input node i, w_{ji} is a scalar called weight between the i^{th} input layer node and j^{th} hidden layer node and b_{jo} is the respective reconstruction error or bias. The output of the hidden layer is given by

$$y_j = f(a_j), \tag{24}$$

where f is the activation function. According to (Bhatti et al., 1996; Rostami et al., 2018), the commonly used activation functions f in practice are: Linear function $a = n$,

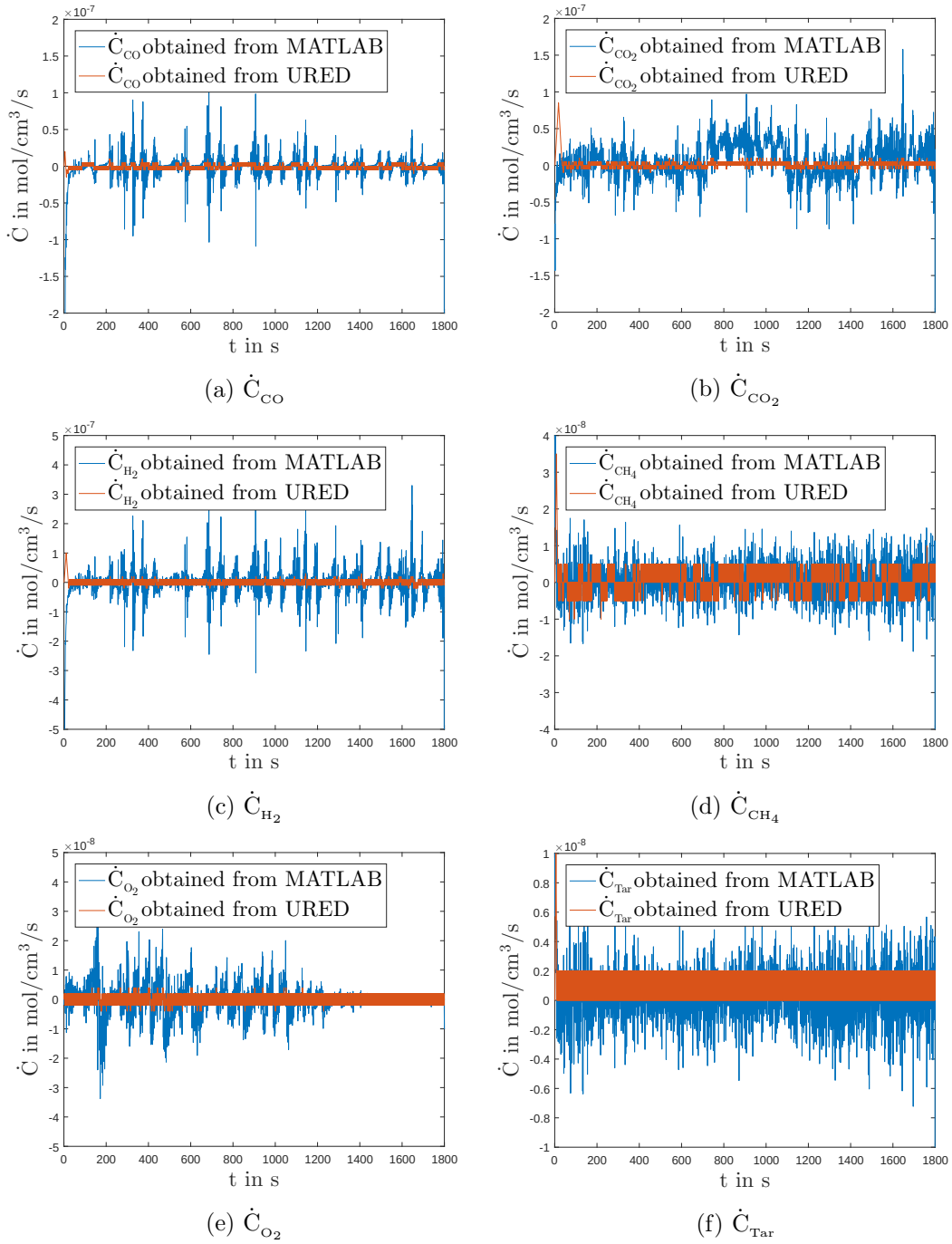

Figure 2. Comparison between the time derivatives of the product gases obtained from Simulink derivative block and URED.

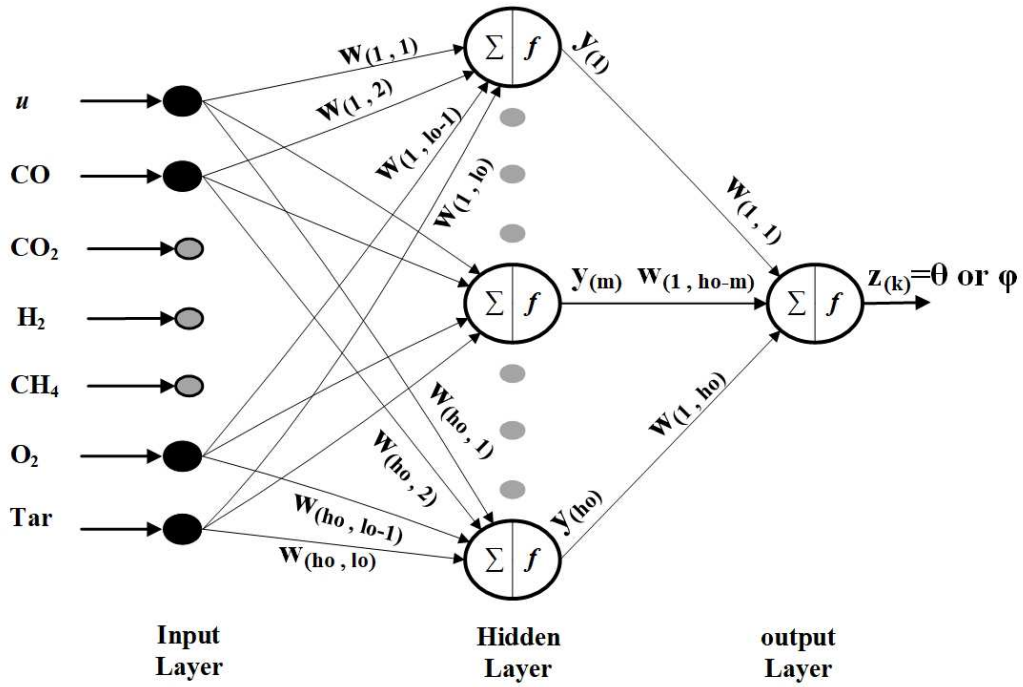

Figure 3. Schematic diagram of MLFFNN for θ or ϕ estimation

Log-sigmoid function $a = \frac{1}{1+e^{-n}}$ and Hyperbolic-tangent sigmoid function $a = \frac{e^n - e^{-n}}{e^n + e^{-n}}$, where n is the number of inputs.

The output layer computes its net activation as follow

$$a_k = \sum_{j=1}^{h_0} w_{kj}\, y_j + b_{k1}, \qquad k = 1, \tag{25}$$

where w_{kj} is a scalar called weight between the k^{th} output layer node and j^{th} hidden layer node. The output layer produces an output as a function of its net activation as follows

$$z_k = f(a_k). \tag{26}$$

The output of the estimated model can be expressed as the function of the inputs, the weights between input and hidden layer and the weights between the hidden and the output layer as described by

$$z_k = f(\sum_{j=1}^{h_0} w_{kj} f(\sum_{i=1}^{l_0} w_{ji}\, p_i + b_{jo}) + b_{k1}). \tag{27}$$

For two layer FFNN as shown in Fig.3, consider l_1 and l_2 are the number of neurons in layer1 and layer2, respectively. So the above equation can also be presented in the

vectors form

$$z_k = f\left(W_2\{f(W_1\bar{p} + b_1)\} + b_2\right), \tag{28}$$

where $\bar{p} \in \Re^{l_1 \times T_s}$, $W_1 \in \Re^{l_1 \times l_0}$, $b_1 \in \Re^{l_1}$, $W_2 \in \Re^{l_2 \times l_1}$, and $b_2 \in \Re^{l_2}$, T_s is the number of input data samples, $\bar{p}$ is the input vector. Same MLFNN architecture is used for both θ and ϕ as shown in Fig. 3 with different hidden layer neurons for obtaining the desired outputs. The Tangent-hyperbolic function is used as a non-linear activation function in the hidden layer, whereas, a linear function is used in the output layer. Depending on the choice of the activation functions the Eq. (28) can be rewritten as

$$z_k = \left(W_2 tanh\{(W_1\bar{p} + b_1)\} + b_2\right). \tag{29}$$

After the selection of the network structure, the network training is done by minimizing the cost function, which is a function of network weights. The cost function is generally characterized as

$$J(w_{ji}, w_{kj}) = \frac{1}{2}\sum_{i=1}^{h_0}(t_k - z_k)^2, \tag{30}$$

where t_k is the target output at the k^{th} output node and $J(w_{ji}, w_{kj})$ is the mean square error (MSE).

Several optimization methods are used for training the network. The most frequently used method is the back propagation learning algorithm (see for instance, (Bhatti et al., 1996; Rostami et al., 2018)).

For updating the weights of NN during training the Levenberg-Marquardt training algorithm (Bhatti et al., 1996; Rostami et al., 2018) is used. The MSE criterion or the maximum number of iterations decide the termination of the iterative process. A range of values of the network parameters has been varied systematically to achieve a good estimate of the training data. The varying network parameters are the number of hidden neurons in the hidden layers (5-50), with learning rate range: 0.1– 0.9 and the number of iterations (50-1000) are used for both the estimation of θ and ϕ. The training flow process is shown in Fig.4.

The final FFNN structure for θ has 20 hidden layer neurons and the learning rate is 0.8. Whereas, for the estimation of ϕ, the learning rate is similar to the previous case, however, 10 hidden layer neurons are used. The choice of the network parameters yields a good match between the actual and the predicted values of the time histories of the variables.

4.2.1. NN Simulation Results

The performance in terms of mean squared error (mse) during the estimation of θ and ϕ is shown in Fig. 5.

The regression plots of θ and ϕ are shown in Fig. 6. The estimates of θ and ϕ are plotted against their corresponding target values in these figures. The regression values of $R = 0.99762$ for θ, and $R = 1$ for ϕ show that the estimates are very close to the target values, indicating the success of FFNN training.

The estimation error histograms associated with θ and ϕ are shown in Fig. 7. It reveals a very small error with an average very close to zero. Finally, the FFNN estimates of θ and ϕ are shown in Fig. 8.

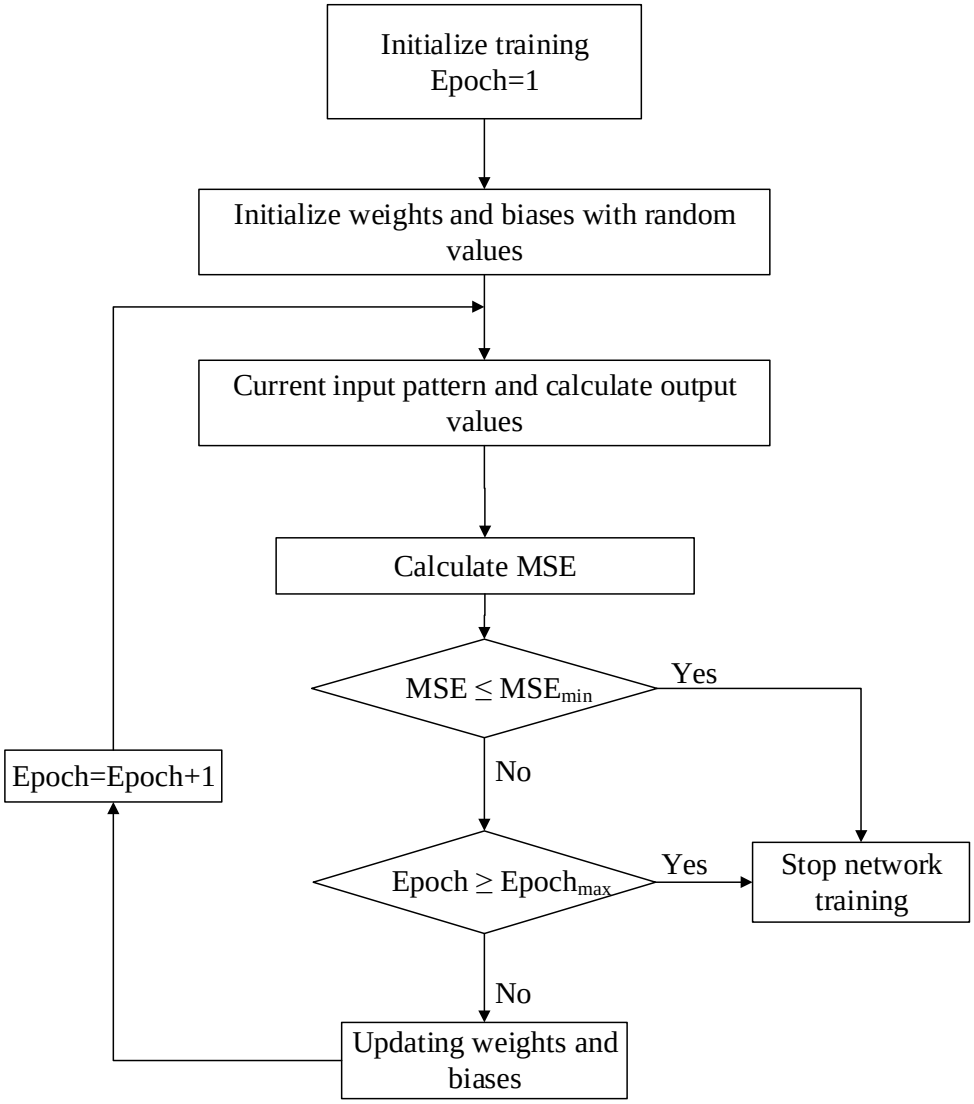

Figure 4. Flowchart for NN training

After properly estimating the functions θ and ϕ, the sliding mode can be enforced by selecting an appropriate value of discontinuous controller gain $\mathcal{K}$. The next section details the implementation of SMC for the UCG process.

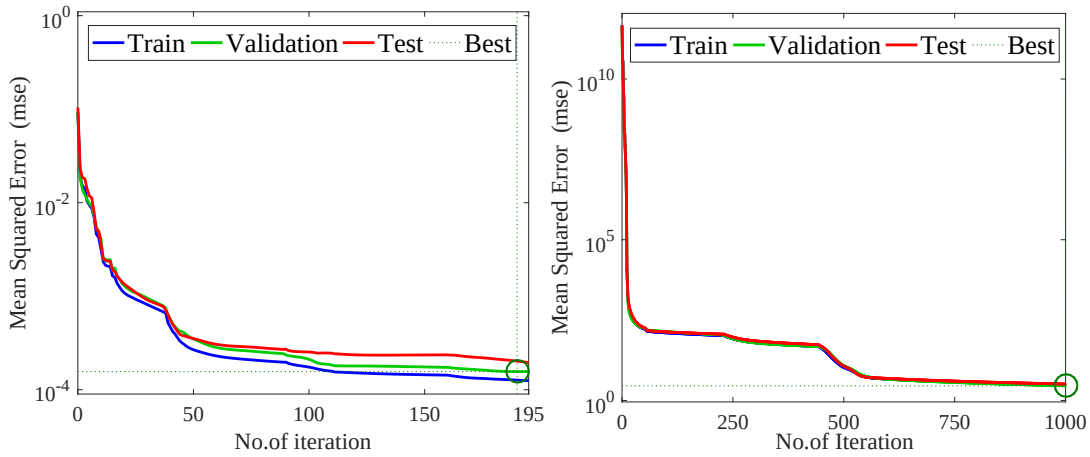

(a) θ (b) ϕ

Figure 5. Mean squared error (MSE) for the estimated parameters

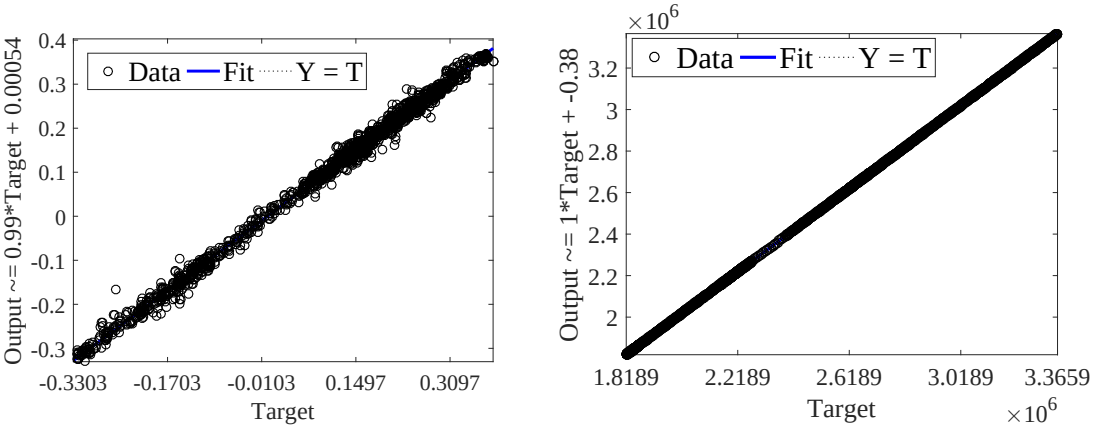

(a) θ (b) ϕ

Figure 6. Estimated and target values of the parameter estimation.

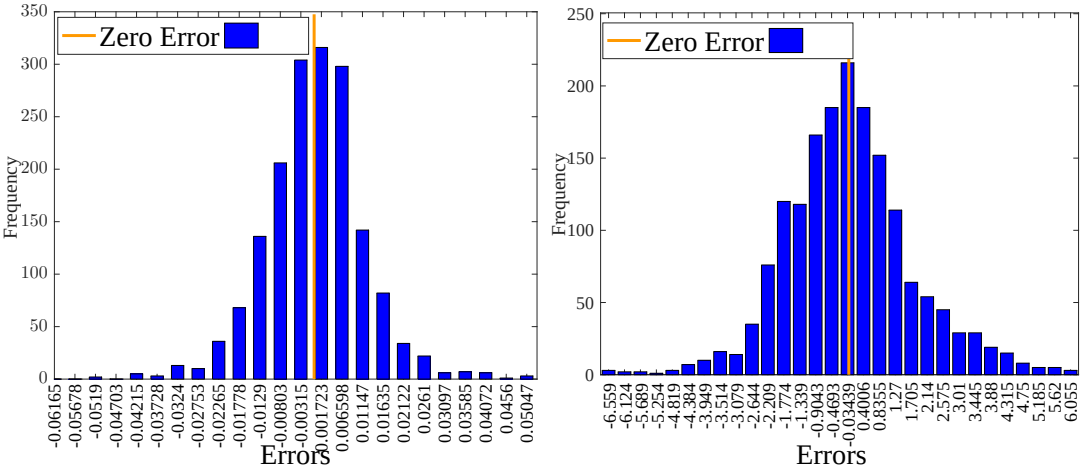

(a) θ (b) ϕ

Figure 7. Error histogram for the estimated parameters.

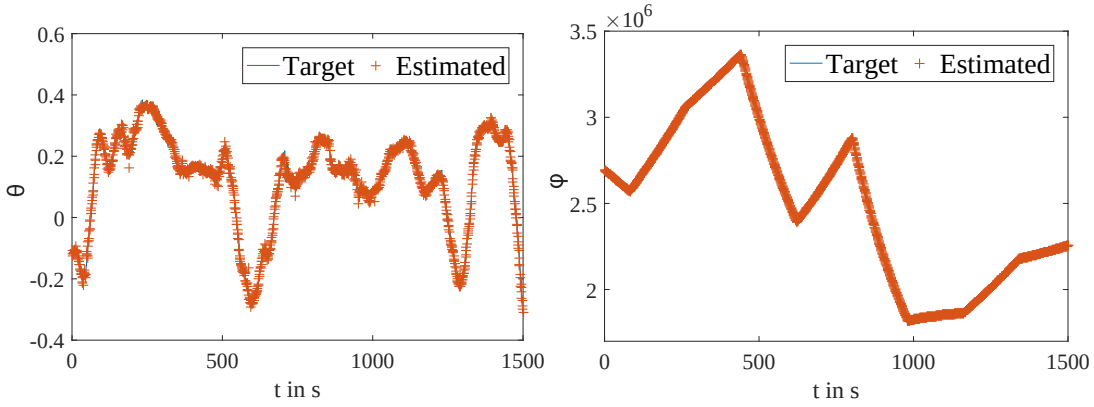

(a) θ (b) ϕ

Figure 8. Estimated and target values of the parameters.

5. Control Implementation Scheme

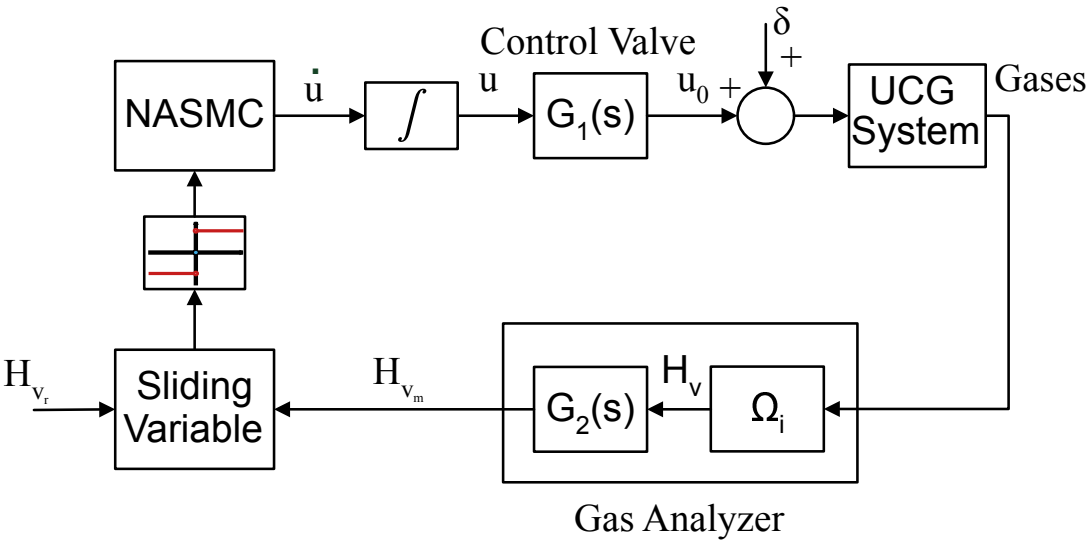

Figure 9. Control implementation strategy

The scheme for controller implementation is adapted from (Uppal et al., 2018a), which is depicted in Fig. 9. It is important to mention that the dynamics of the control valve and the gas analyzer is not considered during the controller design. The transfer functions $G_1(s)$ and $G_2(s)$ represent the dynamics of the control valve and the gas analyzer, respectively, which are modeled as first order systems with time delays (Uppal et al., 2018a). The time delays are approximated with first order Pade's approximation, which results in the following systems

$$G_1(s) = \frac{u_0(s)}{u(s)} = \frac{-\eta_1 s + 2}{(\eta_1 s + 2)(\tau_1 s + 1)}, \tag{31}$$

$$G_2(s) = \frac{H_{v_m}(s)}{H_v(s)} = \frac{-\eta_2 s + 2}{(\eta_2 s + 2)(\tau_2 s + 1)}. \tag{32}$$

where $\eta_i, i \in \{1,2\}$ represents time delays (s), and $\tau_j, j \in \{1,2\}$ are time constants (s) for the control valve and the gas analyzer systems, respectively. Here it is pertinent to mention that the Pade's approximation is used because there is a constant input/output time delay for both the control valve and the gas analyzer systems.

Taking inverse Laplace transform of the Eqs. (31) and (32) yields following second order ODEs

$$\eta_1\tau_1\ddot{u}_0 + (\eta_1 + 2\tau_1)\dot{u}_0 + 2u_0 = -\eta_1\dot{u} + 2u, \tag{33}$$

$$\eta_2\tau_2\ddot{H}_{v_m} + (\eta_2 + 2\tau_2)\dot{H}_{v_m} + 2H_{v_m} = -\eta_2\dot{H}_v + 2H_v. \tag{34}$$

The Eqs. (33) and (34) are numerically solved. The first order time derivatives are approximated by forward Euler's method, whereas, central difference scheme is used for the double time derivatives. The resultant discretized ODEs are given as

$$u_0(t+dt) = \frac{\mathcal{E}u_0(t) + \mathcal{F}u(t) + \mathcal{G}u(t+dt) + \mathcal{H}u_0(t-dt)}{\eta_1 dt + 2dt\tau_1 + \eta_1\tau_1}, \tag{35}$$

$$H_{v_m}(t+dt) = \frac{\mathcal{I}}{P}H_{v_m}(t) + \frac{\mathcal{J}}{P}H_v(t) + \frac{\mathcal{L}}{P}H_v(t+dt) + \frac{\mathcal{M}}{P}H_{v_m}(t-dt), \tag{36}$$

where dt is step size for discretization in time (s), $\mathcal{E} = 2\eta_1\tau_1 + 2dt\tau_1 + dt\eta_1 - 2dt^2$, $\mathcal{F} = 2dt^2 + dt\eta_1$, $\mathcal{G} = -dt\eta_1$, $\mathcal{H} = -\eta_1\tau_1$, $\mathcal{I} = 2\eta_2\tau_2 + 2dt\tau_2 + dt\eta_2 - 2dt^2$, $\mathcal{J} = 2dt^2 + dt\eta_2$, $\mathcal{L} = -dt\eta_2$, $\mathcal{M} = -\eta_2\tau_2$ and $\mathcal{P} = \eta_2 dt + 2dt\tau_2 + \eta_2\tau_2$.

The updated value of the control input $u(t+dt)$ is obtained by the discretization of Eq. (18)

$$u(t+dt) = u(t) - \frac{dt}{\phi(t)}\Big(\mathcal{K}\,\mathrm{sign}(s) + \theta(t)\Big). \tag{37}$$

The NN training is carried out during the open loop operation of the UCG reactor. Furthermore, it can be seen in Fig. 9 that the flow rate of the steam δ produced from the water influx from the aquifers surrounding the UCG reactor acts as an input disturbance. The motivation for considering δ as an input disturbance becomes obvious from Eq. (4), where the vector C_i at the inlet boundary $x = 0$ shows that u and δ enter the system through the same channel. The mechanism for measuring the amount of water intruding in the UCG reactor from the surrounding strata is not available. However, for a successful UCG process, an optimum amount of steam is required (Uppal et al., 2014). The excess steam can decrease the temperature of the reactor, which may slow down the oxidation and gasification reactions responsible for producing the syngas. On the other hand, steam is also a reactant in the main gasification reaction (R_3 in Table. 2), therefore, if the amount of steam drops from a critical value the production of syngas reduces.

The UCG system is numerically solved using the method discussed in (Uppal et al., 2018a). The system is initially operated in the ignition phase, which is followed by the gasification of the coal seam. The coal bed is ignited to increase the temperature of the reactor, so that oxidation and gasification reactions can take place significantly.

The simulation results for NASMC are presented in the following section.

6. Results and discussion

The controller starts operation after the system is operated in the gasification mode for one hour. The closed loop operation is delayed so that the transients of shifting from ignition to gasification phase die out and also H_v may reach a sufficiently higher value. The remainder of the section discusses the simulation results of the closed loop system. Moreover, a fair comparison is also made between the results of NASMC and the conventional SMC design of (Uppal et al., 2018a).

The heating value H_v reaches the desired constant value H_{v_r} (Fig. 10), due to the control input u_0, which is presented in Fig. 11. The time profile of steam flow rate δ at $x = 0$, which is considered as an input disturbance is depicted in Fig. 12. When δ increases between $t = 4$–5 hrs, the amount of steam tends to increase in the reactor, which also elevates the endothermicity of char gasification reaction resulting in the decrease of the reactor temperature. Consequently, the magnitudes of the reaction rates R_1, R_2 and R_3 decrease, which lowers the production of syngas, thereby deteriorating the performance of the process. The controller reacts to the situation by increasing u_0, thus adding more moles of O_2, which catalysis the char oxidation reaction to recover the reactor's temperature and performance. On the other hand when δ decreases between $t = 5$–6 hrs, the molar fraction of steam decreases in the reactor. The controller reduces the concentration of O_2 by lowering down u_0, so that the volumetric content of steam can be restored to facilitate the production of syngas through char gasification reaction. Hence, the NASMC robustly caters the effect of disturbance δ. The sliding variable s, which is the difference between H_{v_r} and H_v is shown in Fig. 13.

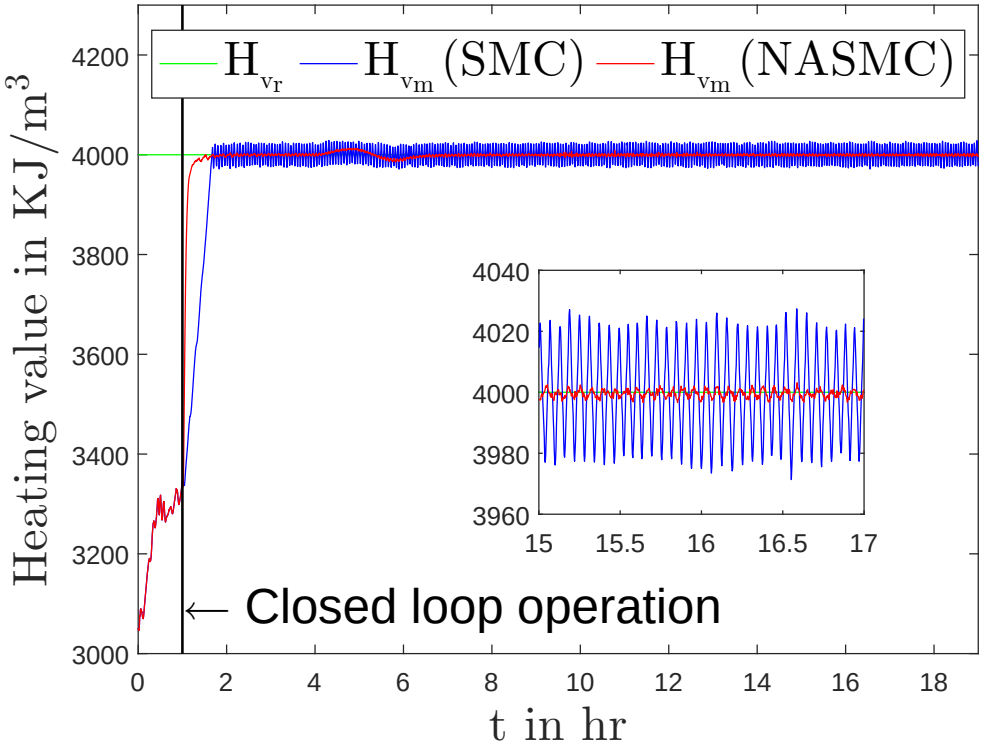

Figure 10. Heating value of the product gases.

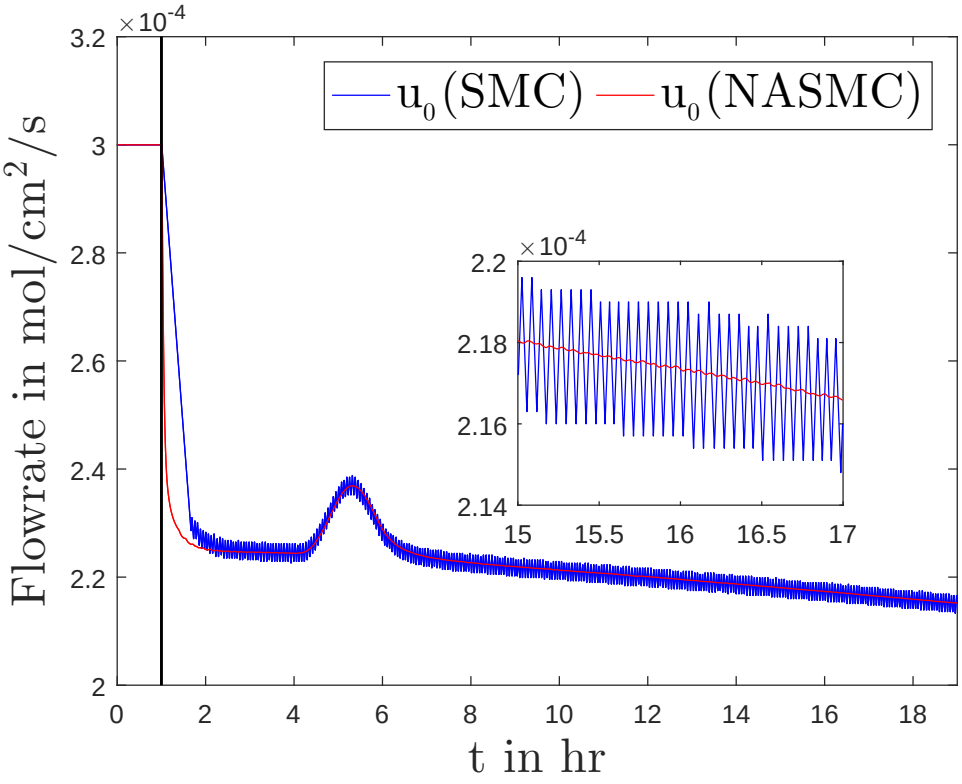

Figure 11. Flow rate of the injected air.

It is obvious from the above results that due to the estimation of the parameters θ and ϕ, the performance of NASMC is more satisfactory and robust as compared to SMC algorithm of (Uppal et al., 2018a).

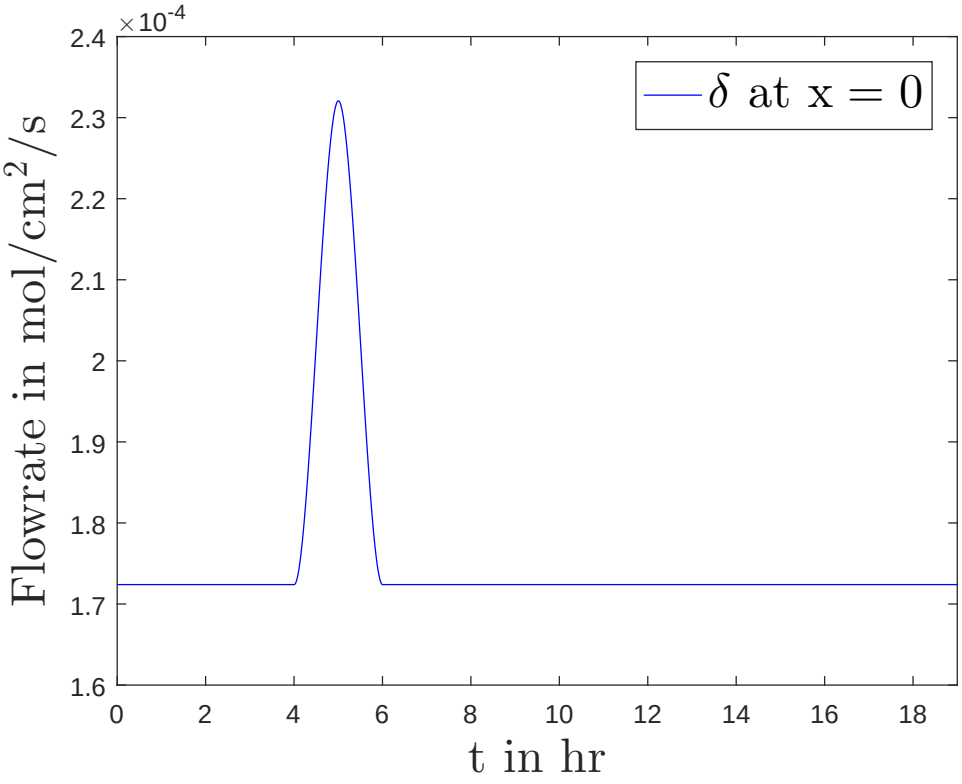

Figure 12. Time profile of input disturbance.

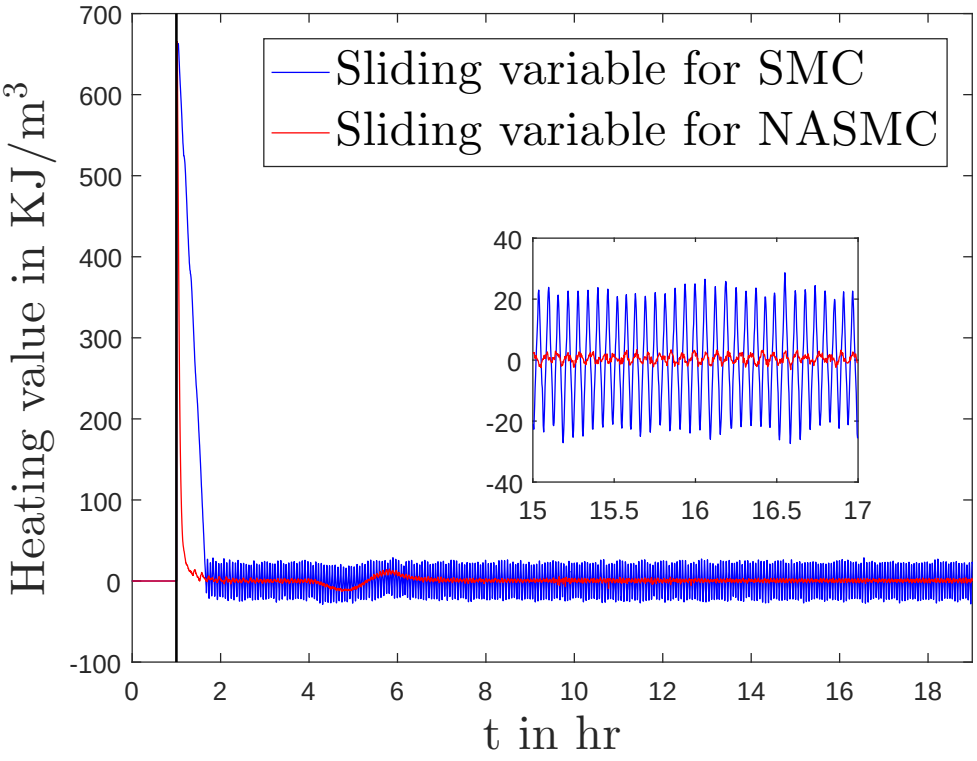

Figure 13. Sliding variable with time.

7. Conclusion

The underground coal gasification problem is formulated as an input output process to maintain a desired heating value of the product gases. Since this problem is subjected to numerous modeling uncertainties and external disturbances, therefore, in this work an NASMC strategy is proposed to provide the necessary robustness. The NNs are used to estimate the unknown state functions and sliding mode is introduced to provide in-sensitivity to modeling imperfections and the disturbance. The target data for NN training requires time derivatives of the measured concentration of the gases, which are estimated via UED. The simulation results demonstrate the effectiveness of the proposed scheme. Moreover, the results obtained from NASMC are compared with the results of the conventional SMC. The comparative results, in nutshell, confirms that NASMC exhibits better performance as compared to its counter part.

References

and and (2002). A fuzzy neural network approximator with fast terminal sliding mode and its applications. In *Proceedings of the 9th International Conference on Neural Information Processing, 2002. ICONIP '02.*, volume 3, pages 1257–1261 vol.3.

Arshad, A., Bhatti, A., Samar, R., Ahmed, Q., and Aamir, E. (2012). Model development of ucg and calorific value maintenance via sliding mode control. In *2012 International Conference on Emerging Technologies (ICET)*, pages 1–6.

Bari, M., Petrovi, I., and Peri, N. (2005). Neural network-based sliding mode control of electronic throttle. *Engineering Applications of Artificial Intelligence*, 18(8):951 – 961.

Bell, D. A., Towler, B. F., and Fan, M. (2011). Chapter 3 - underground coal gasification. In *Coal Gasification and Its Applications*, pages 35 – 71. William Andrew Publishing, Boston.

Bhatti, A., Spurgeon, S., and Lu, X. (1996). Neural network model based indirect sliding mode controller design.

Bouhali, O. and Boudjedir, H. (2011). Neural network control with neuro-sliding mode observer applied to quadrotor helicopter. In *2011 International Symposium on Innovations in Intelligent Systems and Applications*, pages 24–28.

Chairez, I., Poznyak, A., and Poznyak, T. (2006). New sliding-mode learning law for dynamic neural network observer. *IEEE Transactions on Circuits and Systems II: Express Briefs*, 53(12):1338–1342.

Chaudhry, A. M., Uppal, A. A., Alsmadi, Y. M., Bhatti, A. I., and Utkin, V. I. (2018). Robust multi-objective control design for underground coal gasification energy conversion process. *International Journal of Control*, 0(0):1–8.

Chauhan, R. K. and Singh, S. (2017). Application of neural networks based method for estimation of aerodynamic derivatives. In *2017 7th International Conference on Cloud Computing, Data Science Engineering - Confluence*, pages 58–64.

Cruz-Zavala, E., Moreno, J. A., and Fridman, L. M. (2011). Uniform robust exact differentiator. *IEEE Transactions on Automatic Control*, 56(11):2727–2733.

Edwards, C. and Spurgeon, S. (1998). *Sliding Mode Control: Theory And Applications*. Series in Systems and Control. Taylor & Francis.

Ertugrul, M. and Kaynak, O. (2000). Neuro sliding mode control of robotic manipulators. *Mechatronics*, 10(1):239 – 263.

Gautam, P. (2016). System identification of nonlinear inverted pendulum using artificial neural network. In *2016 International Conference on Recent Advances and Innovations in Engineering (ICRAIE)*, pages 1–5.

Ghunem, R. A., Assaleh, K., and El-hag, A. H. (2012). Artificial neural networks with stepwise regression for predicting transformer oil furan content. *IEEE Transactions on Dielectrics and Electrical Insulation*, 19(2):414–420.

Hagan, M. T., Demuth, H. B., and Jesús, O. D. (2002). An introduction to the use of neural networks in control systems. *International Journal of Robust and Nonlinear Control: IFAC-Affiliated Journal*, 12(11):959–985.

Khadse, A., Qayyumi, M., and Mahajani, S. (2006). Reactor model for the underground coal gasification UCG channel. *International Journal of Chemical Reactor Engineering*, 4(1).

Khan, Q. and Akmeliawati, R. (2017). Neuro-adaptive dynamic integral sliding mode control design with output differentiation observer for uncertain higher order mimo nonlinear systems. *Neurocomputing*, 226:126–134.

Kostúr, K. and Kačúr, J. (2008). The monitoring and control of underground coal gasification in laboratory conditions. *Acta Montanistica Slovaca*, 13(1):111–117.

Kostur, K. and Kacur, J. (2011). Development of control and monitoring system of UCG by promotic. In *2011 12th International Carpathian Control Conference (ICCC)*, pages 215 –219.

Kostur, K. and Kacur, J. (2017). Extremum seeking control of carbon monoxide concentration in underground coal gasification. *IFAC-PapersOnLine*, 50(1):13772 – 13777. 20th IFAC World Congress.

Nied, A., Seleme, S., Parma, G., and Menezes, B. (2007). On-line neural training algorithm with sliding mode control and adaptive learning rate. *Neurocomputing*, 70(16):2687 – 2691. Neural Network Applications in Electrical Engineering Selected papers from the 3rd International Work-Conference on Artificial Neural Networks (IWANN 2005).

PARMA, G. G., MENEZES, B. R. D., and BRAGA, A. P. (1999). Neural networks learning with sliding mode control: The sliding mode backpropagation algorithm. *International Journal of Neural Systems*, 09(03):187–193.

Perkins, G. M. P. (2005). *Mathematical Modelling of Underground Coal Gasification*. PhD thesis, The University of New South Wales.

Petroleum, B. (2018). Bp statistical review of world energy june 2018, 2018. *URL: https://www.bp.com/content/dam/bp/en/corporate/pdf/energy-economics/statistical-review/bp-stats-review-2018-full-report.pdf*.

Rostami, A., Anbaz, M. A., Gahrooei, H. R. E., Arabloo, M., and Bahadori, A. (2018). Accurate estimation of co2 adsorption on activated carbon with multi-layer feed-forward neural network (mlfnn) algorithm. *Egyptian Journal of Petroleum*, 27(1):65–73.

Thorsness, C. B. and Rozsa, R. B. (1978). Insitu coal-gasification: Model calculations and laboratory experiments. *Society of Petroleum Engineers Journal*, 18:105–116.

Uppal, A. A. (2016). *Modeling and Control of Underground Coal Gasificatio*. PhD thesis, COMSATS Institute of Information Technology, Islamabad.

Uppal, A. A., Alsmadi, Y. M., Utkin, V. I., Bhatti, A. I., and Khan, S. A. (2018a). Sliding mode control of underground coal gasification energy conversion process. *IEEE Transactions on Control Systems Technology*, 26(2):587–598.

Uppal, A. A., Bhatti, A. I., Aamir, E., Samar, R., and Khan, S. A. (2014). Control oriented modeling and optimization of one dimensional packed bed model of underground coal gasification. *Journal of Process Control*, 24(1):269–277.

Uppal, A. A., Bhatti, A. I., Aamir, E., Samar, R., and Khan, S. A. (2015). Optimization and control of one dimensional packed bed model of underground coal gasification. *Journal of Process Control*, 35:11–20.

Uppal, A. A., Butt, S. S., Bhatti, A. I., and Aschemann, H. (2018b). Integral sliding mode control and gain-scheduled modified utkin observer for an underground coal gasification energy conversion process. In *2018 23rd International Conference on Methods Models in Automation Robotics (MMAR)*, pages 357–362.

Uppal, A. A., Butt, S. S., Khan, Q., and Aschemann, H. (2019). Robust tracking of the heating value in an underground coal gasification process using dynamic integral sliding mode control and a gain-scheduled modified utkin observer. *Journal of Process Control*, 73:113 – 122.

Van der Riet, M. (2008). Underground coal gasification. In *Proceedings of the SAIEE Generation Conference. Eskom College, Midrand (19 Feb 2008)*.

Winslow, A. (1977). Numerical model of coal gasification in a packed bed. *Symposium (International) on Combustion*, 16(1):503 – 513.